A Deformable Surface Model for Vascular Segmentation

Max W.K. Law and Albert C.S. Chung

Lo Kwee-Seong Medical Image Analysis Laboratory,
Department of Computer Science and Engineering,
The Hong Kong University of Science and Technology, Hong Kong
{maxlawwk,achung}@cse.ust.hk

Abstract. Inspired by the motion of a solid surface under liquid pressure, this paper proposes a novel deformable surface model to segment blood vessels in medical images. In the proposed model, the segmented region and the background region are respectively considered as liquid and an elastic solid. The surface of the elastic solid experiences various forces derived from the second order intensity statistics and the surface geometry. These forces cause the solid surface to deform in order to segment vascular structures in an image. The proposed model has been studied in the experiments on synthetic data and clinical data acquired by different imaging modalities. It is experimentally shown that the new model is robust to intensity contrast changes inside blood vessels and thus very suitable to perform vascular segmentation.

1 Introduction

Vascular segmentation is essential to the clinical assessment of blood vessels. To extract vasculatures from medical images, the deformable surface models have been actively studied in the past decade. Lorigo *et al.* have proposed the CURVES algorithm in [1]. CURVES makes use of the minimal curvature to aid the detection of thin vessels. Vasilevskiy and Siddiqi [2] have introduced the image gradient-flux to deform surfaces for the segmentation of vascular structures. The image gradient-flux encapsulates both the image gradient magnitude and direction. It is capable of detecting small and low contrast vasculatures. Rochery *et al.* have devised the higher order active contour model in [3]. The higher order active contour model factors in the image intensity, the geometry of target structures and the contour smoothness to extract tubular structures. Klein *et al.* [4] have presented the use of a B-Spline based deformable surface model to segment vessels. Yan and Kissim have elaborated the capillary action [5] for segmentation of vessels. The capillary force aims at pulling the evolving surface into thin and low contrast vessels. Nain *et al.* devised the shape driven flow [6] to reduce the chance of false positive detection when segmenting vessels.

In this paper, a novel deformable surface model is proposed. The deformable surface can be viewed as the surface of an elastic solid (the background region)

G.-Z. Yang et al. (Eds.): MICCAI 2009, Part II, LNCS 5762, pp. 59–67, 2009.

that is in contact with the liquid (the segmented region). The surface is represented as a level set function. It experiences forces derived from the second order intensity statistics and the surface geometry. These forces are related by the force equilibrium equation of a solid-liquid interface [7]. The dynamics of the surface are governed by the net force acting on the surface. The surface deformation equation can inspect the second order intensity change along the surface tangential plane as well as the surface normal direction. It helps deform the surface to propagate through the position where changes of object intensity contrast happen.

The proposed model is studied using a synthetic and numerical image volume. It is also compared against a well founded vascular segmentation approach, the CURVES algorithm [1], by using the clinical datasets consisting of three different imaging modalities. It is experimentally shown that the proposed model is suitable to perform segmentation of vascular structures.

2 Methodology

2.1 The Proposed Model

In the proposed model, the segmented region and the background region are respectively regarded as liquid and an elastic solid (Fig. 1). As such, the solid surface is the boundary that separates the segmented region and the background region. There are three kinds of forces acting on the solid surface. First, the liquid exerts pressure on the solid surface. Second, the surface of the elastic solid has surface stress which opposes the change of the surface area of the solid. Third, an external bulk stress is acted on the surface of the solid. These forces are derived based on the second order intensity variation and the geometry of the solid surface. Given P is the pressure exerted by the liquid, $\mathbf{s}$ and $\mathbf{B}$ are symmetric tensors which represent the surface stress force and the bulk stress force at the solid surface respectively, at the force equilibrium position, these forces are related as [7],

$$(P - \mathrm{div}_{\mathbf{S}}\mathbf{s})\boldsymbol{n} + \mathbf{B}\boldsymbol{n} = \mathbf{0}, \tag{1}$$

where $\mathrm{div}_{\mathbf{S}}$ is surface divergence and $\boldsymbol{n}$ is the inward surface normal of the solid.

By placing an initial surface inside the target vessels, the proposed model allows the solid surface to deform according to the net force acting on it. This aims at seeking the force equilibrium position of the surface. Denote $\mathcal{C}$ be the solid surface, the change of the surface with respect to time t is determined by the net force acting on the surface,

$$\mathcal{C}_{\mathbf{t}} = (P - \mathrm{div}_{\mathbf{S}}\mathbf{s})\boldsymbol{n} + \mathbf{B}\boldsymbol{n}. \tag{2}$$

The liquid pressure and the bulk stress experienced by the solid surface are devised based on the second order intensity statistics, which are widely used for the detection of vasculatures [8] [9] [10]. The pressure exerted by the liquid

is defined as $P = -\Delta I$. Inside tubular structures, the Laplacian responses are negative and with large magnitudes. A large negative Laplacian response results in a high liquid pressure inside tubular structures to push the solid surface. On the other hand, the bulk stress acting on the solid surface $\mathbf{B}$ is defined as the negative second order intensity change along the surface normal, i.e. $\mathbf{B} = -\alpha I_{\boldsymbol{nn}} \boldsymbol{n}\boldsymbol{n}^T$, where α determines the strength of the stress force. Since the second order intensity changes are large along the vessel cross-sectional planes, and small along the vessel direction, this bulk stress force intends to pull the solid along the vessel cross-sectional planes.

The second order intensity change magnitudes decrease at the positions away from the vessel centers and thus, the stress force as well as the liquid pressure decline accordingly. The bulk stress and the liquid pressure finally become small or vanish at the vessel boundaries. The surface receives very small or no force at the vessel boundaries where the deformation of the surface is therefore stopped at the vessel boundaries. Besides, the surface stress of the solid which opposes to the change of the solid surface area is designed to be constant and isotropic. As discussed in Section 2.3, such a constant and isotropic surface stress leads to a smooth resultant surface. Given $\boldsymbol{u}$ and $\boldsymbol{v}$ are two arbitrary orthogonal tangential directions of the surface, the tensor of the constant and isotropic surface stress can be written as, $\mathbf{s} = \gamma[\boldsymbol{u}\ \ \boldsymbol{v}][\boldsymbol{u}\ \ \boldsymbol{v}]^T$, where γ controls the surface stress strength.

Assigning the aforementioned forces to Eqn. 2, we have $\mathcal{C}_\mathbf{t} = (-\Delta I - \mathrm{div}_s(\gamma[\boldsymbol{u}\ \ \boldsymbol{v}][\boldsymbol{u}\ \ \boldsymbol{v}]^T))\boldsymbol{n} - \alpha I_{\boldsymbol{nn}} \boldsymbol{n}\boldsymbol{n}^T$. Since $\Delta I = \mathrm{Tr}(\mathbf{H})$ and $\mathrm{div}_\mathrm{S}([\boldsymbol{u}\ \ \boldsymbol{v}][\boldsymbol{u}\ \ \boldsymbol{v}]^T) = -2\kappa\boldsymbol{n}$ [11] for the Euclidean mean curvature of the surface κ,

$$\mathcal{C}_\mathbf{t} = (-\mathrm{Tr}([\boldsymbol{u}\ \ \boldsymbol{v}]^T\mathbf{H}[\boldsymbol{u}\ \ \boldsymbol{v}]) + 2\gamma\kappa)\boldsymbol{n} - (1+\alpha)(I_{\boldsymbol{nn}}\boldsymbol{n}\boldsymbol{n}^T)\boldsymbol{n}. \tag{3}$$

For the simplicity of discussion, denote $\gamma' = 2\gamma$, $\alpha' = 1 + \alpha$, $\mathbf{G}(\mathbf{H}; \boldsymbol{n}) = (\boldsymbol{n}^T\mathbf{H}\boldsymbol{n})(\boldsymbol{n}\boldsymbol{n}^T) = I_{\boldsymbol{nn}}\boldsymbol{n}\boldsymbol{n}^T$, $\mathbf{M} = \begin{bmatrix} I_{uu} & I_{uv} \\ I_{uv} & I_{vv} \end{bmatrix} = \begin{bmatrix} \boldsymbol{u}^T\mathbf{H}\boldsymbol{u} & \boldsymbol{u}^T\mathbf{H}\boldsymbol{v} \\ \boldsymbol{u}^T\mathbf{H}\boldsymbol{v} & \boldsymbol{v}^T\mathbf{H}\boldsymbol{v} \end{bmatrix} = [\boldsymbol{u}\ \ \boldsymbol{v}]^T\mathbf{H}[\boldsymbol{u}\ \ \boldsymbol{v}]$,

$$\mathcal{C}_\mathbf{t} = (-\mathrm{Tr}(\mathbf{M}) + \gamma'\kappa)\boldsymbol{n} - \alpha'\mathbf{G}(\mathbf{H}; \boldsymbol{n})\boldsymbol{n}. \tag{4}$$

2.2 Vessel Specific Image Features and Multiscale Detection

If the surface is deforming along a vessel, the surface tangential plane is equivalent to the cross-sectional plane of the vessel. The eigenvalues of $\mathbf{M}$ would be negative and with large magnitudes. Furthermore, vessels are mainly in tubular shape with roughly circular cross-sections. Therefore, the ratio and the signs of these two eigenvalues are exploited to suppress the surface deformation speed in the structures producing non-negative eigenvalues or large difference between the two eigenvalues. The surface deformation equation (Eqn. 4) is refined as $\mathcal{C}_\mathbf{t} = (-f(\mathbf{H}; \boldsymbol{u}, \boldsymbol{v}) + \gamma'\kappa)\boldsymbol{n} - \alpha'\mathbf{G}(\mathbf{H}; \boldsymbol{n})\boldsymbol{n}$, and

$$f(\mathbf{H}; \boldsymbol{u}, \boldsymbol{v}) = \begin{cases} \mathrm{Tr}(\mathbf{M}) \exp\left(1 - \frac{\xi_2}{\xi_1}\right) & \text{if } \xi_1 < 0 \text{ and } \xi_2 < 0, \\ 0 & \text{otherwise,} \end{cases} \tag{5}$$

where ξ_1 and ξ_2 are the eigenvalues of $\mathbf{M}$ and $|\xi_1| \leq |\xi_2|$.

Since vessel sizes vary in practice, the second order intensity statistics are computed on the images smoothed by Gaussian kernels with various scales (defined by the value of σ as shown in Fig. 2a) for multiscale detection. The scales are sampled logarithmically as discussed by Sato *et al.* in [10]. Suppose the Hessian matrix obtained at the scale σ is $\mathbf{H}^{\sigma}$ and the associated Hessian matrix along the surface is $\mathbf{M}^{\sigma}$, the surface deformation equation becomes,

$$\mathcal{C}_{\mathbf{t}} = -f(\mathbf{H}^{\arg\max_{\sigma}|\mathrm{Tr}(\mathbf{M}^{\sigma})|}; \boldsymbol{u}, \boldsymbol{v})\boldsymbol{n} - \alpha'\mathbf{G}(\mathbf{H}^{\arg\max_{\sigma}|\boldsymbol{n}^T\mathbf{H}^{\sigma}\boldsymbol{n}|}; \boldsymbol{n})\boldsymbol{n} + \gamma'\kappa\boldsymbol{n}, \quad (6)$$

where the terms $\arg\max_{\sigma}|\mathrm{Tr}(\mathbf{M}^{\sigma})|$ and $\arg\max_{\sigma}|\boldsymbol{n}^T\mathbf{H}^{\sigma}\boldsymbol{n}|$ select the scales that exhibit the largest second order intensity changes along the surface tangential plane and along the surface normal, among a set of pre-defined scales.

The solid surface is represented as the zero boundaries of the level set function [12]. The evolution of the level set function was implemented according to the description by Whitaker [13] and based on the Insight-Toolkits [14]. The level set function evolution was stopped when the change of the level set function was less than 0.0001 per segmented voxel over 40 evolution iterations. When the level set function is evolving, $\mathbf{H}$ in one scale is obtained in a $3*3*3$ local window by taking central difference on one buffered image, which is Gaussian-smoothed before the evolution begins. $\mathbf{M}$ is retrieved from $\mathbf{H}$ and the surface tangents $\boldsymbol{u}$ and $\boldsymbol{v}$. Bilinear interpolation is used at the positions with non-integer coordinates. This procedure is repeated for each scale. The complexity of evaluating Eqn. 6 for one voxel is linear with respect to the number of scales used.

2.3 Properties of the Proposed Model

The function $f(\cdot)$ (Eqn. 5) has a large magnitude when the eigenvalues are negative, with large and similar magnitudes. This corresponds to the scenario that the surface is deforming along the vessel, as illustrated in Case 1 of Figs. 2b-d. In Cases 2 and 3 of Figs. 2b-d, the magnitudes of either one of or both of the eigenvalues of $\mathbf{M}^{\sigma}$ are small. In such cases, the resultant values of $f(\cdot)$ are suppressed by the exponential term. The surface is deformed according to the second and the third terms in the right hand side of Eqn. 6. The surface beyond vessel boundaries in Case 2 and the solid surface approaching the vessel boundary in Case 3 are expanded and shrunk respectively, according to the value of $\boldsymbol{n}^T\mathbf{H}\boldsymbol{n}$. The surface is in turn converged to the vessel boundary. Besides, Case 4 of Fig. 2 corresponds to the situation that the surface reaches the vessel boundary and the second order intensity variations along all directions are small. The deforming surface is therefore halted at the vessel boundary.

Regarding the parameters of the proposed model, the solid stress strength α' is used to specify how much the second order intensity change along the surface normal influences the speed of surface deformation. A small value of α' reduces the surface deformation speed induced by the second order intensity change along the surface normal. It causes the surface deforming aggressively along tubular structures. Enlarging the value of α' increases the chance of detecting non-tubular structures, such as, high curvature vessels or junctions. On the other

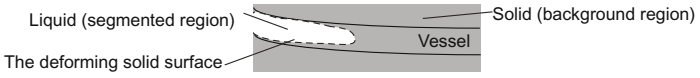

Fig. 1. The proposed deformable surface model

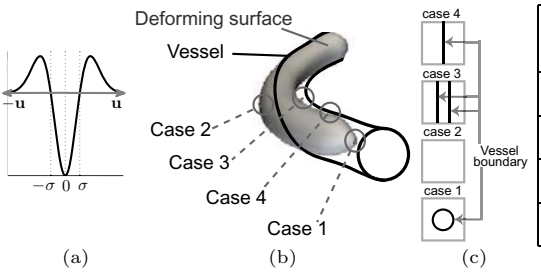

(a) (b) (c)

Case no. and description of the surface	$\boldsymbol{n}^T\mathbf{H}\boldsymbol{n}$	ξ_1	ξ_2
1, deforming along vessel	≈ 0	$\xi_1 \approx \xi_2 \ll 0$	
2,deforming beyond vessel boundary	> 0	≈ 0	≈ 0
3, approaching vessel boundary	< 0	≈ 0	< 0
4, at vessel boundary	≈ 0	≈ 0	≈ 0

(d)

Fig. 2. (a) A plot of the second derivative of a Gaussian function along $\boldsymbol{u}$. (b) An example showing various situations when the surface is deforming to segment a vessel. (c) The surface tangential planes in different cases in (b). The black lines show the positions where the vessel boundary crosses the tangential planes. (d) The descriptions of various terms appeared in the definitions of $f(\cdot)$ and $\mathbf{G}(\cdot)$. σ is assumed to be the same as the vessel radius.

hand, the surface stress term of the solid (the third term in the right hand side of Eqn. 6) is analogous to the curvature regularization term which is commonly utilized in active contour methods. The value of γ' determines the smoothness of the resultant surface.

As the proposed model makes use of a 2D-circular-constraint (Eqn. 5), it exhibits extra flexibility on handling branches as compared to Hessian based methods which have a more restrictive 3D-tubular-constraint. Meanwhile, the proposed method inspects the second order intensity changes along the surface tangential plane and the surface normal direction separately. This makes our method more robust when the vessel intensity contrast varies rapidly along the vessel. The rapid change of vessel contrast can be caused by image noise or closely located objects with intensity similar to the vessels. A rapid change of vessel intensity contrast can significantly alter the directions of the image gradient and the principle directions of the Hessian matrix. It can undesirably terminate the deformation of the moving surface inside vessels in some deformable surface models, which are grounded on the image gradient [1][5] or the Hessian matrix [15]. For the proposed model, the intensity variations are measured along the directions defined by the deforming surface. When the surface is deforming along and inside vessels, the surface tangential plane at the evolving tip of the surface is equivalent to the vessel cross-sectional plane. Inspecting the intensity changes along the surface tangential plane is therefore able to capture the second order intensity changes along vessel cross-sectional plane. It consequently keeps the surface deforming along vessel despite of the rapid change of intensity contrast.

Fig. 3. The synthetic and numerical image volume with the size of $20 \times 20 \times 60$ voxels, consists of a vertical tube with a radius of 2 voxels. (a) The $x = 10$ slice of the image volume. (b) The intensity values in different parts of the image volume. (c) The initial surface. (d-f) The surface deformation results of $\mathcal{C}_\mathbf{t} = -f(\mathbf{H}^{\arg\max_\sigma |\mathrm{Tr}(\mathbf{M}^\sigma)|}; \boldsymbol{u}, \boldsymbol{v})\boldsymbol{n}$; $\mathcal{C}_\mathbf{t} = -\mathbf{G}(\mathbf{H}^{\arg\max_\sigma |\boldsymbol{n}^T\mathbf{H}^\sigma\boldsymbol{n}|}; \boldsymbol{n})\boldsymbol{n}$; the proposed model using $\alpha' = 1$ and $\gamma' = 0$.

3 Experimental Results

The proposed method is validated by using four volumetric images: a numerical image volume consisting of a synthetic tube (Fig. 3a), an intracranial phase contrast magnetic resonance angiographic (PCMRA) image[1](Fig. 4a), an intracranial time-of-flight magnetic resonance angiographic (TOFMRA) image [1](Fig. 4d) and a cardiac computed tomographic angiographic (CTA) image [2](Fig. 4g).

3.1 Synthetic Data

In this section, we employ a synthetic tube (Figs. 3a and b) which exaggerates a rapid change of intensity contrast along a vessel. With this rapid change of vessel intensity contrast, we demonstrate the behavior of the term involving the second order intensity change along the surface tangential plane, and the term involving the second order intensity change along surface normal in the surface deformation equation. These two terms are $f(\cdot)\boldsymbol{n}$ and $\mathbf{G}(\cdot)\boldsymbol{n}$ in Eqn. 6 respectively.

In this experiment, an initial surface is placed at the bottom of the tube (Fig. 3c). Two resultant surfaces are obtained by deforming this initial surface according to $\mathcal{C}_\mathbf{t} = -f(\mathbf{H}^{\arg\max_\sigma |\mathrm{Tr}(\mathbf{M}^\sigma)|}; \boldsymbol{u}, \boldsymbol{v})\boldsymbol{n}$ and $\mathcal{C}_\mathbf{t} = -\mathbf{G}(\mathbf{H}^{\arg\max_\sigma |\boldsymbol{n}^T\mathbf{H}^\sigma\boldsymbol{n}|}; \boldsymbol{n})\boldsymbol{n}$. Five logarithmic scale samples are taken from the range of 1 to 5 voxel length. The resultant surfaces are shown in Figs. 3d and e respectively. Since the surface tangential plane at the evolving tip corresponds to the vessel cross-sectional plane, the deforming surface can propagate through the position where the tube intensity contrast changes. However, it cannot segment the entire tube as $f(\cdot)$ is small or zero when the surface tangential plane does not correspond to the vessel cross-sectional plane, where ξ_1 and ξ_2 are not both negative and with similar magnitudes (see Eqn. 5).

[1] Acquired using a Philips 3T ACS Gyroscan MR scanner without the use of contrast agent, at the University Hospital of Zurich, Switzerland.

[2] Rotterdam Coronary Artery Algorithm Evaluation Framework, "http://coronary.bigr.nl/"

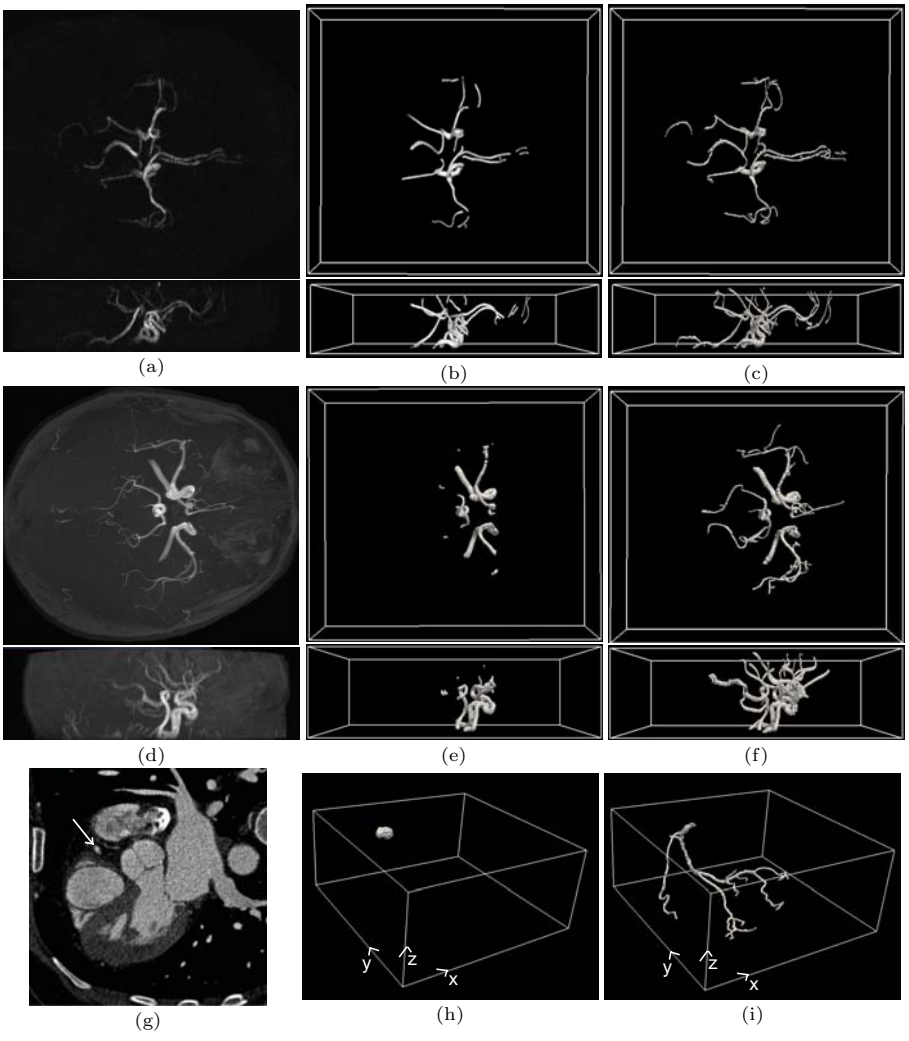

Fig. 4. (a, d, g) The three clinical datasets used in the experiments, an intracranial PCMRA image with $512 \times 512 \times 46$ voxels and voxel size of 0.39mm×0.39mm×0.8mm; an intracranial TOFMRA image with $512 \times 512 \times 60$ voxels and voxel size of 0.39mm×0.39mm×0.95mm; and the $z = 190$ slice of a cardiac CTA image with $512 \times 512 \times 190$ voxels and voxel size of 0.34mm×0.34mm×0.4mm, the white arrow points at the position where the initial surface/contour is placed. (b, e, h) The segmentation results using the CURVES algorithm. (c, f, i) The segmentation results using the proposed method.

Besides, in Fig. 3e, the deforming surface is halted by the rapid change of intensity contrast. Finally, by making use of both $f(\cdot)\boldsymbol{n}$ and $\mathbf{G}(\cdot)\boldsymbol{n}$, deforming the surface based on Eqn. 6 can segment the entire tube Fig. 3f, despite of the large change of tube intensity contrast.

3.2 Clinical Data

We have applied both our method and the CURVES algorithm [1] to segment the vasculatures in the three clinical datasets (Figs. 4a, d, g). The initial surface and contour of the proposed method and CURVES in the first and the second cases are obtained by thresholding the regions with 0.5% of the highest intensity in the entire image. In the CTA dataset, a single-voxel region manually placed in the right coronary artery is employed as the initial surface for the proposed method and the initial contour for CURVES. Five scale samples are obtained analogous to the synthetic experiment for the multiscale detection of the proposed model. The values of the parameters α' and γ' are 0.75 in all cases. For CURVES, in each dataset, we only show the segmented region which gives no leakage and that region has the largest number of segmented voxels among those obtained using various parameter values in the evolution equation of CURVES.

Comparing Figs. 4b and c, the proposed method is capable of segmenting more vessels in the PCMRA image. The main reason is that the analysis of the second order intensity variation along the surface tangential plane helps the surface deform along vessels, despite the present of intensity contrast variations along vascular structures. In the TOFMRA image and the CTA image, we have found that the evolving contours of CURVES leak frequently at the boundaries where adjacent tissues with intensity similar to vessels present. CURVES could only segment a small portion of the vessels (see Figs. 4e and h) before leakages happen. Besides, the proposed method has no problem to extract the vasculatures from the TOFMRA and the CTA images (Figs. 4f and i).

4 Discussion and Conclusion

The surface dynamics described in Eqn. 2 is a simplified case of the motion of a solid surface under liquid pressure in practice [16]. For instance, in the proposed model, the solid surface is assumed to be purely elastic and the bonding between the atoms on the solid surface does not break during deformation. Nevertheless, the proposed model based on the simplified deformation dynamic of the solid surface well serves the purpose of segmentation of vessels. Meanwhile, handling stenoses or aneurysms, and quantitative evaluation for a specific applications will be the future research directions of this work.

In summary, this paper proposes a novel physics-based deformable surface model for segmenting blood vessels in medical images. By considering the second order intensity statistics as various forces acting on the deforming surface, the proposed method allows the surface to propagate along vessels despite the presence of undesired intensity contrast fluctuations along vessels. The proposed method has been studied in the experiments using synthetic data, and compared with a classic deformable surface model, the CURVES algorithm [1], in the experiments using medical images acquired by various imaging modalities. It is demonstrated that the proposed method is well suited to segment vasculatures from medical images.

References

1. Lorigo, L., Faugeras, O., Grimson, W., Keriven, R., Kikinis, R., Nabavi, A., Westin, C.: Curves: Curve evolution for vessel segmentation. MedIA 5(3), 195–206 (2001)
2. Vasilevskiy, A., Siddiqi, K.: Flux maximizing geometric flows. PAMI 24(12), 1565–1578 (2002)
3. Rochery, M., Jermyn, I., Zerubia, J.: Higher order active contours. IJCV 69(1), 27–42 (2006)
4. Klein, A., Lee, F., Amini, A.: Quantitative coronary angiography with deformable spline models. TMI 16(5), 468–482 (1997)
5. Yan, P., Kassim, A.: Segmentation of volumetric mra images by using capillary active contour. MedIA 10(3), 317–329 (2006)
6. Nain, D., Yezzi, A., Turk, G.: Vessel segmentation using a shape driven flow. In: Barillot, C., Haynor, D.R., Hellier, P. (eds.) MICCAI 2004. LNCS, vol. 3216, pp. 51–59. Springer, Heidelberg (2004)
7. Weissmuller, J., Kramer, D.: Balance of force at curved solid metal - liquid electrolyte interfaces. Langmuir 21(10), 4592–4603 (2005)
8. Frangi, A., Niessen, W., Viergever, M.: Multiscale vessel enhancement filtering. In: Wells, W.M., Colchester, A.C.F., Delp, S.L. (eds.) MICCAI 1998. LNCS, vol. 1496, pp. 130–137. Springer, Heidelberg (1998)
9. Koller, T., Gerig, G., Szekely, G., Dettwiler, D.: Multiscale detection of curvilinear structures in 2-d and 3-d image data. In: IEEE International Conference on Computer Vision, pp. 864–869 (1995)
10. Sato, Y., Nakajima, S., Shiraga, N., Atsumi1, H., Yoshida, S., Koller, T., Gerig, G., Kikinis, R.: Three-dimensional multi-scale line filter for segmentation and visualization of curvilinear structures in medical images. MedIA 2(2), 143–168 (1998)
11. Gurtin, M., Weissmuller, J., Larche, F.: A general theory of curved deformable interfaces in solids at equilibrium. Philosophical Magazine 78(5), 1093–1109 (1998)
12. Malladi, R., Sethian, J., Vemuri, B.: Shape modeling with front propagation: A level set approach. PAMI 17(2), 158–175 (1995)
13. Whitaker, R.: A level-set approach to 3d reconstruction from range data. IJCV 29(33), 203–231 (1998)
14. Ibanez, L., Schroeder, W., Ng, L., Cates, J.: The ITK Software ToolKit
15. Descoteaux, M., Collins, L., Siddiqi, K.: Geometric flows for segmenting vasculature in MRI: Theory and validation. In: Barillot, C., Haynor, D.R., Hellier, P. (eds.) MICCAI 2004. LNCS, vol. 3216, pp. 500–507. Springer, Heidelberg (2004)
16. Kramer, D., Weissmuller, J.: Note on surface stress and surface tension and their interrelation via shuttleworth's equation and the lippmann equation. Surf. Sci. 601(14), 3042–3051 (2007)